Article

Solution-Based II#VI Core/Shell Nanowire Heterostructures

Jim A. Goebl, Robert W. Black, James Puthussery, Jay Giblin, Thomas H. Kosel, and Masaru Kuno

J. Am. Chem. Soc., **2008**, 130 (44), 14822-14833 • DOI: 10.1021/ja805538p • Publication Date (Web): 11 October 2008

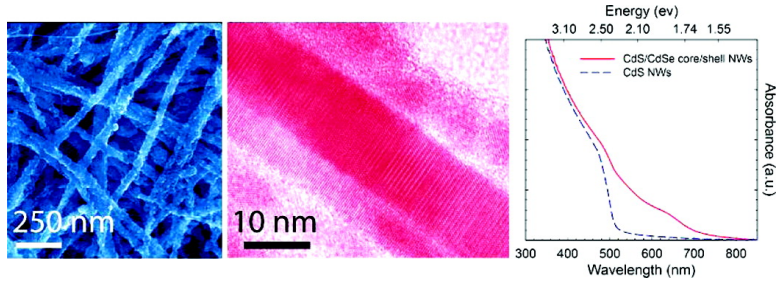

More About This Article

Additional resources and features associated with this article are available within the HTML version:

- Supporting Information
- Access to high resolution figures
- Links to articles and content related to this article
- Copyright permission to reproduce figures and/or text from this article

View the Full Text HTML

J|A|C|S
ARTICLES

Published on Web 10/11/2008

Solution-Based II−VI Core/Shell Nanowire Heterostructures

Jim A. Goebl,[†] Robert W. Black,[†,§] James Puthussery,[†] Jay Giblin,[†] Thomas H. Kosel,[‡] and Masaru Kuno*[,†]

Department of Chemistry and Biochemistry and Notre Dame Radiation Laboratory, Department of Electrical Engineering, University of Notre Dame, Notre Dame, Indiana 46556, and Nanotechnology Engineering, University of Waterloo, Waterloo, Ontario, Canada, N2L 3G1

Received July 24, 2008; E-mail: mkuno@nd.edu

Abstract: We demonstrate the solution-phase synthesis of CdS/CdSe, CdSe/CdS, and CdSe/ZnTe core/shell nanowires (NWs). On the basis of bulk band offsets, type-I and type-II heterostructures are made, contributing to the further development of low-dimensional heteroassemblies using solution-phase chemistry. Core/shell wires are prepared by slowly introducing shell precursors into a solution of premade core NWs dispersed in a noncoordinating solvent at moderate temperatures (215−250 °C). Resulting heterostructures are characterized through low- and high-resolution transmission electron microscopy, selected area electron diffraction, and energy dispersive X-ray analysis. From these experiments, initial shell growth appears to occur through either Stranski−Krastanov or Volmer−Weber island growth. However, beyond a critical shell thickness, nucleation of randomly oriented nanocrystals results in a polycrystalline coat. In cases where overcoating has been achieved, corresponding elemental analyses show spatially varying compositions along the NW radial direction in agreement with expected element ratios. Electronic interactions between the core and shell were subsequently probed through optical studies involving UV−vis extinction spectroscopy, photoluminescence experiments, and transient differential absorption spectroscopy. In particular, transient differential absorption studies reveal unexpected shell-induced changes in core NW Auger kinetics at high carrier densities. Previously seen three-carrier Auger kinetics in CdS (bimolecular in CdSe) NWs were suppressed by the presence of a CdSe (CdS) shell. These observations suggest the ability to influence NW optical/electrical properties by coating them with a surrounding shell, a method which could be important for future NW optical studies as well as for NW-based applications.

1. Introduction

Semiconductor nanowires (NWs) are of great scientific interest because their intrinsic optical and electrical properties make them amenable for uses in photovoltaics,[1] electronics,[2] and sensors.[3] They also exhibit potential confinement effects which open up avenues for directly manipulating their optical/electrical properties.[4] In addition, dielectric contrast effects offer the tantalizing possibility of manipulating the electronic response of NWs through changes in their local dielectric environment.[5] Furthermore, band structure engineering has been explored by inducing strain within the NW system, resulting in observed piezoelectric effects[6] as well as tunable emission energies.[7−9] Current challenges in NW synthesis therefore revolve around developing cost-effective methods for controlling wire growth as well as creating more complex heterostructures exhibiting above-mentioned confinement, dielectric contrast, and strain-engineered effects to better manipulate their optical and electrical response.

In this regard, solution-based syntheses such as solution−liquid−solid (SLS) growth[10−12] show promise for achieving both thermodynamic and kinetic control over NW crystallization. This parallels trends seen in the colloidal growth of analogous zero-dimensional (0D) materials such as quantum dots (QDs, alternatively called nanocrystals, NCs) where high-quality particles with narrow size distributions and tunable sizes have been made by employing high-boiling solvents in conjunction

[†] Department of Chemistry and Biochemistry and Notre Dame Radiation Laboratory, University of Notre Dame.
[‡] Department of Electrical Engineering, University of Notre Dame.
[§] University of Waterloo.

(1) Tian, B.; Zheng, X.; Kempa, T.; Fang, Y.; Yu, N.; Yu, G.; Huang, J.; Lieber, C. M. *Science* **2007**, *449*, 885.
(2) Ma, R.-M.; Dai, L.; Huo, H.-B.; Xu, W.-J.; Qin, G. G. *Nano Lett.* **2007**, *7*, 3300.
(3) Patolsky, F.; Timko, B. P.; Yu, G. H.; Fang, Y.; Greytak, A. B.; Zheng, G. F.; Lieber, C. M. *Science* **2006**, *313*, 1100.
(4) Gudiksen, M. S.; Wang, J.; Lieber, C. M. *J. Phys. Chem. B* **2002**, *106*, 4036.
(5) Muljarov, E. A.; Zhukov, E. A.; Dneprovskii, V. S.; Masumoto, Y. *Phys. Rev. B* **2000**, *62*, 7420.
(6) Lin, H. M.; Chen, Y. L.; Yang, J.; Liu, Y. C.; Yin, K. M.; Kai, J. J.; Chen, F. R.; Chen, L. C.; Chen, Y. F.; Chen, C. C. *Nano Lett.* **2003**, *3*, 537.
(7) Zanolli, Z.; Froberg, L. E.; Bjork, M. T.; Pistol, M.-E.; Samuelson, L. *Thin Solid Films* **2006**, *515*, 793.
(8) Skold, N.; Karlsson, L. S.; Larsson, M.; Pistol, M.-E.; Seifert, W.; Tragardh, J.; Samuelson, L. *Nano Lett.* **2005**, *5*, 1943.
(9) Schrier, J.; Demchenko, D.; Wang, L. W.; Alivisatos, A. P. *Nano Lett.* **2007**, *7*, 2377.
(10) Wang, F.; Dong, A.; Sun, J.; Tang, R.; Yu, H.; Buhro, W. E. *Inorg. Chem.* **2006**, *45*, 7511.
(11) Kuno, M. *Phys. Chem. Chem. Phys.* **2008**, *10*, 620.
(12) (a) Grebinski, J. W.; Richter, K. J.; Zhang, J.; Kosel, T. H.; Kuno, M. *J. Phys. Chem. B* **2004**, *108*, 9745. (b) Grebinski, J. W.; Hull, K. J.; Zhang, J.; Kosel, T. H.; Kuno, M. *Chem. Mater.* **2004**, *16*, 5260. (c) Kuno, M.; Ahmad, O.; Protasenko, V.; Bacinello, D.; Kosel, T. H. *Chem. Mater.* **2006**, *18*, 5722. (d) Puthussery, J.; Lan, A.; Kosel, T. H.; Kuno, M. *ACS Nano* **2008**, *2*, 357.

 10.1021/ja805538p CCC: $40.75

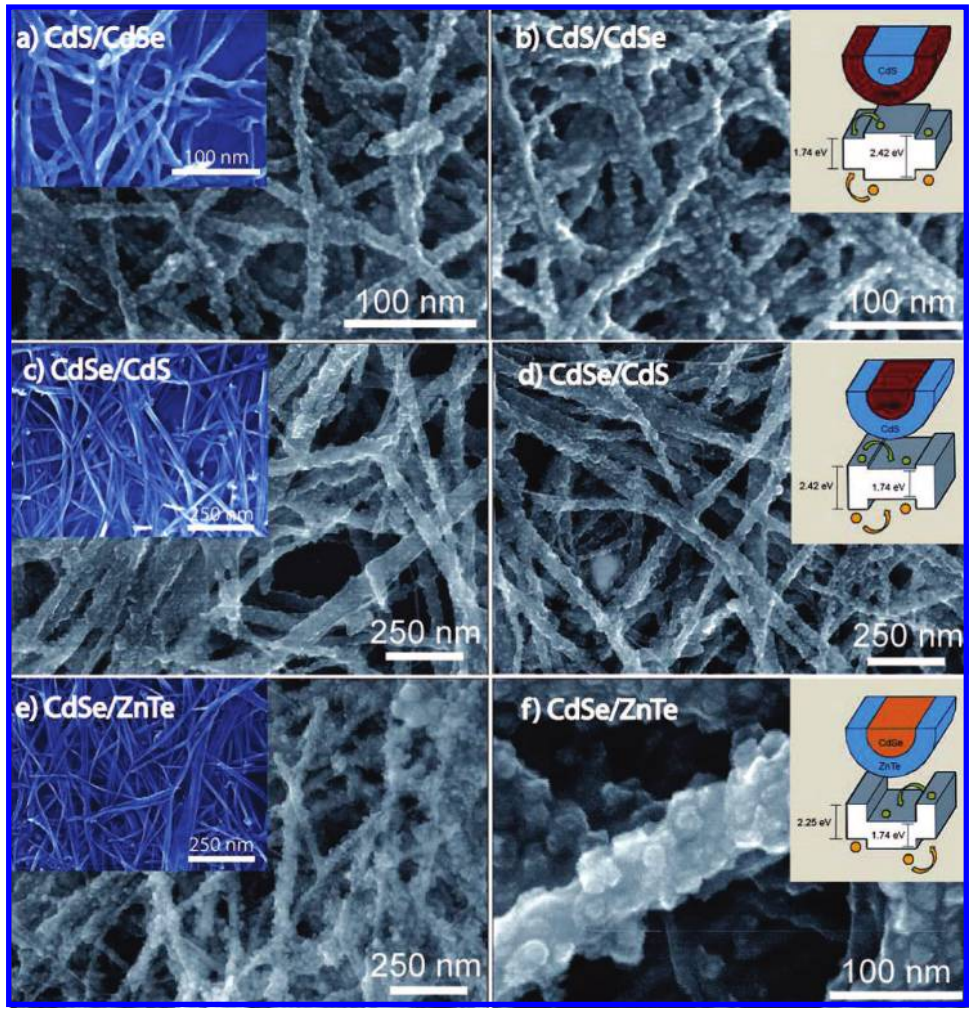

Figure 1. SEM images of (a and b) CdS/CdSe, (c and d) CdSe/CdS, (e and f) CdSe/ZnTe core/shell NWs. Accompanying insets on the left show core NWs before overcoating. Insets on the right depict the band offsets potentially present in each system based on bulk values.

with coordinating/noncoordinating surfactants.[13,14] In tandem, numerous solution-based approaches exist for creating more complex NC structures, exhibiting rodlike[15,16] and other higher-order morphologies.[17] These latter materials have been made by carefully manipulating nanostructure growth kinetics through the use of metal/chalcogen coordinating ligands.

Complex core/shell heterostructures have also been made using solution chemistry. This entails coating NCs with a shell of another semiconductor to enhance emission quantum yields[18−20] and/or charge separation capabilities.[21,22] Although various chemical vapor deposition (CVD) based approaches exist for creating analogous core/shell (coaxial) NW heterostructures,[23−26] few examine methods for creating such assemblies in solution.[27,28] In the following study, we therefore demonstrate the synthesis of such core/shell NWs through the slow introduction of precursors into a mixture of premade NWs dispersed in a noncoordinating solvent.

Three core/shell systems, CdS/CdSe, CdSe/CdS, and CdSe/ZnTe, were developed and are illustrated schematically in the inset of Figure 1. On the basis of bulk electron affinities,

(13) (a) Peng, X. *J. Am. Chem. Soc.* **2002**, *124*, 3343. (b) Peng, X.; Wickham, J.; Alivisatos, A. P. *J. Am. Chem. Soc.* **1998**, *120*, 5343.
(14) Murray, C. B.; Norris, D. J.; Bawendi, M. G. *J. Am. Chem. Soc.* **1993**, *115*, 8706.
(15) Peng, X.; Manna, L.; Yang, W. D.; Wickham, J.; Scher, E.; Kadavanich, A.; Alivisatos, A. P. *Nature* **2000**, *404*, 59.
(16) Kan, S. H.; Mokari, T.; Rothenberg, E.; Banin, U. *Nat. Mater.* **2003**, *2*, 155.
(17) (a) Milliron, D. J.; Hughes, S.; Cui, Y.; Manna, L.; Li, J.; Wang, L. W.; Alivisatos, A. P. *Nature* **2004**, *430*, 190. (b) Salman, A.; Tortschanoff, A.; Mohamed, M. B.; Tonti, D.; Mourik, F.; Chergui, M. *Appl. Phys. Lett.* **2007**, *90*, 093104.
(18) Hines, M. A.; Guyot-Sionnest, P. *J. Phys. Chem.* **1996**, *100*, 468.
(19) Dabbousi, B. O.; Rodriguez-Viejo, J.; Mikulec, F. V.; Heine, J. R.; Mattoussi, H.; Ober, R.; Jensen, K. F.; Bawendi, M. G. *J. Phys. Chem. B* **1997**, *101*, 9463.
(20) Peng, X.; Schlamp, M. C.; Kadavanich, A. V.; Alivisatos, A. P. *J. Am. Chem. Soc.* **1997**, *119*, 7019.
(21) Aharoni, A.; Mokari, T.; Popov, I.; Banin, U. *J. Am. Chem. Soc.* **2006**, *128*, 257.
(22) Kim, S.; Fisher, B.; Eisler, H. J.; Bawendi, M. *J. Am. Chem. Soc.* **2003**, *125*, 11466.
(23) Hsu, Y.-J.; Lu, S.-Y.; Lin, Y.-F. *Adv. Funct. Mater.* **2005**, *15*, 1350.
(24) (a) Lauhon, L. J.; Gudiksen, M. S.; Wang, D.; Lieber, C. M. *Nature* **2002**, *420*, 57. (b) Tian, B.; Zheng, X.; Kempa, T. J.; Fang, Y.; Yu, N.; Yu, G.; Huang, J.; Lieber, C. M. *Nature* **2007**, *449*, 885.
(25) (a) Skold, N.; Karlsson, L. S.; Larsson, M. W.; Pistol, M.-E.; Seifer, W.; Tragardh, J.; Samuleson, L. *Nano Lett.* **2005**, *5*, 1943. (b) Zanolli, Z.; Pistol, M.-E.; Froberg, L. E.; Samuelson, L. *J. Phys.: Condens. Matter* **2007**, *19*, 1.
(26) Law, M.; Greene, L. E.; Radenovic, A.; Kuykendall, T.; Liphardt, J.; Yang, P. D. *J. Phys. Chem. B* **2006**, *110*, 22652.
(27) Talapin, D. V.; Yu, H.; Shevchenko, E. V.; Lobo, A.; Murray, C. B. *J. Phys. Chem. C* **2007**, *111*, 14049.
(28) Dong, A.; Wang, F.; Dalton, T. L.; Buhro, W. E. *Nano Lett.* **2007**, *7*, 1308.

heterostructures with both type-I and type-II band offsets have been made. Tabulated literature values of corresponding bulk band offsets can be found in the Supporting Information. In the case of CdS/CdSe, the lower (higher) CdSe conduction (valence) band position relative to CdS suggests that any photogenerated electrons and holes will preferentially migrate into the shell. By the same token, reversing the composition of the core and the shell creates a structure where a confining potential exists for both electrons and holes. This may, in turn, improve NW emission quantum yields (QYs) by suppressing carrier access to surface states.[18−20] Finally, in the case of CdSe/ZnTe core/shell heterostructures, a staggered band offset is expected with both ZnTe conduction and valence bands above those of CdSe. This could theoretically promote the spatial separation of electrons and holes upon photogeneration and could be useful for photovoltaic applications. Furthermore, tunable emission energies within the red and infrared are possible.[22]

In tandem, given that relatively few studies have been conducted on the optical properties of core/shell NWs, the current study also focuses on their optical response primarily within the context of transient differential absorption experiments. Specifically, such experiments were conducted to see the influence of the shell on the intraband/interband relaxation kinetics of the NWs. In principle, the existence of band offsets could lead to changes in carrier relaxation dynamics due to carrier migration from the core into the shell or vice versa. This would then add to growing studies about relaxation mechanisms within NWs and, in particular, about their Auger decay kinetics.[12c,29]

In general, such solution-based core/shell NWs illustrate extensions of solution-phase heterostructure growth to one-dimensional (1D) NWs. Subsequent optical studies conducted on them may improve our understanding about basic NW optical/electrical properties and may also aid their use in various applications given the potential for dielectric contrast engineering, the enhancement of NW QYs, and the possibility of interface-driven charge separation. Furthermore, strain engineering may enable one to manipulate their band structure.[7−9] At the same time, the development of core/shell heterostructures may lead to the eventual remote doping of solution-based NWs in a manner akin to the modulation doping of bulk semiconductors.[30]

2. Materials and Methods

2.1. Materials. Toluene, methanol, and hexanes were used as received from Fisher Scientific. In the synthesis of CdS and CdSe NWs, trioctylphosphine oxide (TOPO, 99%, Aldrich), cadmium oxide (CdO, 99%, Aldrich), oleic acid (90%, Aldrich), trioctylphosphine (TOP, 90%, Aldrich), tributylphosphine (TBP, 97%, Aldrich), oleylamine (OLA, TCI America), squalane (99%, Acros), octadecene (ODE, 90%, Aldrich), diethylzinc ($ZnEt_2$, 99.999%, Strem), bis(trimethylsilyl)sulfide [$(TMS)_2S$, <95%, Fluka], and bis(trimethylsilyl)selenide [$(TMS)_2Se$, Gelest] were all purchased and used as received. Dimethylcadmium ($CdMe_2$, 99.995%, Strem) was passed through a 0.2 μm PTFE filter in a glovebox and was stored at low temperature.

Tellurium powder (200 mesh, 99.8%, Aldrich) was used to prepare tributylphosphine telluride (TBPTe, ~1 M) by mixing 2.56 g (5 mmol) with TBP (20 mL, 80 mmol) in a glovebox and allowing the mixture to stir overnight. The resulting solution was filtered through a 0.2 μm PTFE syringe filter to yield a clear yellow solution. Selenium (sulfur) powder, 99.5+%, Aldrich (99.999%, Acros), was used to prepare trioctylphosphine selenide (TOPSe, 1 M) [trioctylphosphine sulfide (TOPS, 2 M)] by mixing known amounts of selenium (1.58 g, 20 mmol) [sulfur (1.282 g, 40 mmol)] with TOP (20 mL, 44.8 mmol) and allowing the resulting solution to stir overnight.

Au/Bi catalyst particles for NW synthesis were made using a procedure described in ref 12a. Briefly, ligand-passivated Au nanoparticles (NPs) were synthesized with an average diameter of 1.5 nm and a corresponding size distribution of 18%. NPs were subsequently dissolved in toluene and one-quarter of this sample was placed in a mixture of phenyl ether and TOP. A solution consisting of 30 μL (0.184 mmol) $Bi(Et)_3$ in TOP was added dropwise at 100 °C to produce Au NPs with a thin Bi shell. Resulting particles were then washed and resuspended in toluene. A small amount of oleic acid was added to the final product to prevent particle aggregation. Catalyst NPs were finally refrigerated in an inert atmosphere glovebox to suppress any unwanted oxidation.

2.1.1. Synthesis of Straight CdS NWs. Straight CdS NWs were synthesized using a modified procedure based on that outlined in ref 12d. Briefly, CdO (0.0648 g, 0.5 mmol), oleic acid (90%, 0.4 mL, 1.26 mmol), and squalane (5 mL, 9.58 mmol) were heated under vacuum at ~100 °C to dry and degas the mixture. The reaction vessel was back-filled with N_2 and was heated to 290 °C. Simultaneously, a solution of ~1.5 nm diameter Au/Bi NPs (200 μL, ~76 nmol), and 1 M TOPS (1.5 mL, 1.5 mmol) was prepared in a glovebox and was loaded into a 5 mL disposable syringe. When the temperature of the reaction mixture reached 290 °C, the prepared solution was injected into the Cd containing mixture. After a brief induction period, its color rapidly changed from clear to dark orange, indicating CdS NW growth. The reaction vessel was kept at high temperature for approximately 2 min before being cooled to room temperature.

2.1.2. Synthesis of Straight CdSe NWs. Straight CdSe NWs were synthesized using a previously reported procedure[12b] with slight modifications. Briefly TOPO (2.5 g, 6.46 mmol), CdO (0.025 g, 0.194 mmol), and octanoic acid (0.23 mL, 1.43 mmol) were added to a three-neck flask with a condenser and a thermocouple. The flask was then connected to a Schlenk line where the solution was dried and degassed under vacuum at ~100 °C. When complete, the reaction vessel was back-filled with N_2 and was heated to 360 °C. The solution eventually became clear, whereupon two separate syringes, one containing ~1.5 nm diameter Au/Bi NPs (230 μL, 87.4 nmol) and the other 1 M TOPSe (25 μL, 25 μmol), were prepared inside a glovebox. These solutions were then injected into the reaction mixture, yielding an immediate color change from clear to red/brown. This indicates the formation of CdSe NWs. The resulting solution was then left at high temperature for approximately 2 min before being cooled to room temperature.

2.1.3. Processing. Once both NW solutions reached ~70 °C, an excess of toluene (~10 mL) was added to the mixture. Wires were then extracted by adding methanol (~10−15 mL), followed by centrifuging the resulting suspension. Recovered wires were then redispersed in toluene. Additional methanol could be added to reprecipitate the wires, and subsequent centrifuging was used to extract them. This "washing" procedure was repeated two more times to remove as much excess (surface-bound) surfactant as possible. In the case of CdSe NWs, the final precipitate was resuspended in pyridine. The addition of a large excess of this weakly coordinating ligand aids in removing TOPO from the NW surface and is important since the latter surfactant strongly adheres to the wire. Pyridine-dispersed CdSe NWs were precipitated using a nonpolar solvent, such as hexane. This pyridine washing step was repeated two more times. An analogous pyridine washing step was not required for CdS NWs since noncoordinating solvents were

(29) Robel, I.; Bunker, B.; Kamat, P. V.; Kuno, M. *Nano Lett.* **2006**, *6*, 1344.
(30) Kroemer, H. *Surf. Sci.* **1986**, *174*, 299.

used in their synthesis. Both CdSe and CdS NWs were ultimately resuspended in toluene and stored for future use.

NW stock solution concentrations were "standardized" through their UV−vis extinction spectra. Concentrations were estimated using theoretical absorption cross sections (Supporting Information) as well as previous experimental values.[31] Note that the employed approximation is formally valid only at frequencies far to the blue of the band edge where the NW density of states becomes bulklike. As a consequence, factor of 2 cross section errors can easily exist at the band edge as suggested by comparisons between experiment and theory in ref 31. In the case of CdSe wires, a NW concentration of 5.77×10^{-11} M was obtained for 100 μL of stock diluted in 3 mL of toluene. The corresponding absorbance was 0.17 at 650 nm (1.91 eV). An identical procedure was carried out with CdS NWs, yielding typical stock concentrations of 7.06×10^{-10} M for 200 μL of stock diluted in 3 mL of toluene. The corresponding absorbance was 0.23 at 480 nm (2.58 eV).

2.1.4. NW Thermal Stability. To prepare for subsequent overcoating experiments, the thermal stability of core (alternatively, "bare") NWs was investigated. Both CdS and CdSe NWs were dispersed in ODE, and resulting suspensions were heated to 290 °C for 90 min. No noticeable change in the color or physical appearance of NW solutions was observed, corroborated by additional UV−vis extinction and TEM experiments. Processed NWs were therefore stable at temperatures suitable for overcoating, in slight contrast to nanorods (NRs).[32]

2.1.5. Synthesis of CdS/CdSe Core/Shell NWs. Approximately 0.5 mL ($\sim 3.39 \times 10^{-13}$ mol) of a known CdS NW stock solution was added to ODE (5 mL, 15.6 mmol) in a three-neck flask connected to a Schlenk line. The mixture was heated under vacuum at ~100 °C to dry and degas it. Once complete, the vessel was back-filled with N_2 and the temperature was raised to 240 °C. At this point, an "injection" solution consisting of TBP (1.81 mL, 7.2 mmol), $CdMe_2$ (7.0 μL, 97.2 μmol), and 1 M TOPSe (0.19 mL, 0.19 mmol) was loaded into a 20 mL disposable syringe inside a glovebox. When the temperature of the reaction mixture stabilized, the solution was introduced into the three-neck flask at a controlled rate of 10 mL/h [486 (950) μmol/h metal (chalcogen)] using a syringe pump. The color of the NW suspension changed from light yellow to amber during addition. Once complete, the mixture was cooled to 70 °C and NWs were extracted by centrifuging the suspension with an excess of toluene. No additional methanol was required. Recovered wires were then cleaned by centrifuging the precipitate with additional toluene three times. All final precipitates were resuspended in toluene and stored for future use.

2.1.6. Synthesis of CdSe/CdS Core/Shell Nanowires. The overcoating procedure for CdSe NWs is nearly identical to that outlined above with the following differences. A known amount of CdSe NWs (~0.5 mL, $\sim 2.90 \times 10^{-14}$ mol) was placed in a three-neck flask with 5 mL of squalane (9.58 mmol). Precursors in the overcoating solution include $CdMe_2$ (4.5 μL, 62.5 μmol) and $(TMS)_2S$ (5 μL, 23.7 μmol) dissolved in squalane (2.5 mL, 4.79 mmol). These reagents were loaded into a disposable 20 mL syringe inside a glovebox. Once the temperature of the NW containing reaction mixture stabilized at 250 °C, the overcoating stock was introduced at a controlled rate of ~10 mL/h [250 (94.8) μmol/h metal (chalcogen)] using a syringe pump. During injection, the color of the NW mixture changed from light brown to dark orange. Workup of the resulting product was identical to that for CdS/CdSe NWs.

2.1.7. Synthesis of CdSe/ZnTe Core/Shell Nanowires. This synthesis also mimics the overcoating of CdS NWs, with the following changes. A known amount of CdSe NWs (~0.5 mL, $\sim 2.90 \times 10^{-14}$ mol) was placed in a three-neck flask with 3 mL of ODE (9.38 mmol). Two equal volume injection solutions of metal and chalcogen were prepared in separate 20 mL syringes to prevent an undesired reaction between the two. The metal solution contained $ZnEt_2$ (8 μL, 78.1 μmol) diluted in TOP (2.5 mL, 5.61 mmol), while the chalcogen solution contained 1 M TBPTe (0.2 mL, 0.2 mmol) also diluted in TOP (2.3 mL, 5.20 mmol). When the temperature of the reaction mixture stabilized at 240 °C, both solutions were simultaneously introduced into the reaction vessel at a rate of ~5 mL/h [156 (400) μmol/h metal (chalcogen)] using two syringe pumps. The color of the NW mixture changed from light brown to pale yellow. Workup of the resulting product was identical to the procedure described above. When exposed to air, the color of the recovered material gradually turned black. This color change was suppressed by keeping the overcoated wires in an inert atmosphere glovebox, suggesting that the effect stems from oxidation of the NW surface. However, subsequent elemental analyses proved inconclusive, leaving the origin of the color change undetermined.

2.2. Instrumentation. Resulting core/shell NWs were studied using transmission electron microscopy (TEM). Preliminary TEM micrographs were acquired with a JEOL 100SX TEM. Additional low- and high-resolution TEM micrographs were taken with a JEOL 2010 TEM operating at 200 kV. The 2010 is outfitted with an X-ray detector to enable energy-dispersive X-ray spectroscopy (EDXS) measurements of the NW elemental composition. Scanning electron microscopy (SEM) was also performed on resulting core/shell NWs using a Hitachi S-4500 field emission scanning electron microscope.

All UV−vis extinction spectra for CdS and CdSe NWs as well as their overcoated counterparts were obtained at room temperature with a Cary 50-Bio UV−vis spectrophotometer. NW solutions were prepared by diluting known amounts of a given stock with toluene. A 1 cm path length Suprasil cuvette was used in all experiments. Baseline corrections were conducted prior to each measurement. Emission experiments were conducted using a home-built single-molecule imaging microscope coupled to a fiber-based spectrometer (Ocean Optics) and CCD. NW QYs were estimated through a comparison to individual dye-doped polystyrene beads of known QY. More information about the instrument can be found in ref 33. Excitation sources included a 405 nm diode laser as well as the wavelength selected output of a supercontinuum white light source (Fianium).

Ultrafast transient differential absorption experiments were performed with a Clark MXR CPA 2010 laser system employing a fiber-based spectrometer. Samples were excited with the second harmonic (387 nm, 3.2 eV) of the fundamental, a fraction of which was passed through a sapphire plate to generate a white light continuum between 420 and 800 nm (1.5−2.9 eV). An optical delay line provided probe delays between 150 fs and 1.6 ns. Samples were prepared by embedding NWs in poly(methyl methacrylate) (PMMA, 15 000 MW). Typical optical densities ranged from 0.06 to 0.1 at 680 nm. Corresponding pump fluences ranged from 23.9 to 120 μJ/cm^2. All acquired spectra were chirp-corrected.

3. Results and Discussion

3.1. Synthesis. SEM images of resulting core/shell NWs are shown in Figure 1. From these micrographs, an apparent transition from bare starting NWs (left inset) to the final core/shell material is evident. The images further suggest that the syntheses described above (Materials and Methods) overcoat ~90% of core wires with a relatively uniform shell across their length.

For various reasons, different overcoating procedures were needed for NWs relative to QDs. Although the overcoating of colloidal QDs is relatively straightforward and entails adding precursors of a desired shell material to NCs dispersed in coordinating[18−20,22,34,35] or noncoordinating[21,36] solvents, a

(31) Protasenko, V.; Bacinello, D.; Kuno, M. *J. Phys. Chem. B* **2006**, *110*, 25322.
(32) Mokari, T.; Banin, U. *Chem. Mater.* **2003**, *15*, 3955.
(34) Mekis, I.; Talapin, D. V.; Kornowski, A.; Haase, M.; Weller, H. *J. Phys. Chem. B* **2003**, *107*, 7454.

direct translation to NWs does not appear to work. Specifically, the primary consideration for overcoating QDs is the slow and dilute addition of precursors at moderate temperatures to prevent the self-nucleation of shell elements. This, in turn, favors their deposition onto the surface of existing NCs. By contrast, NWs do not exhibit the same core/shell permissibility, for reasons that are unclear. To overcome this issue, synthetic parameters were deliberately altered to explore the viability of making core/shell NWs. Results of these investigations are outlined below and enable one to formulate a qualitative understanding of the eventual synthesis developed.

The first important realization was that, in general, noncoordinating solvents were strongly preferred when overcoating NWs. This was determined by attempts to overcoat NWs in solvents with varying coordinating abilities. They include, from coordinating to noncoordinating, TOPO, OLA, phenyl ether, octyl ether, ODE, and squalane. Of these, only those procedures utilizing ODE or squalane yielded coatings for all three NW heterostructures. Furthermore, ODE was favored over squalane for CdS/CdSe and CdSe/ZnTe preparations, since the latter often led to very rough coatings and solutions containing unwanted byproducts. For the CdSe/CdS system, however, squalane was the only solvent which worked successfully. Procedures using ODE left the wires uncoated.

We speculate that, since noncoordinating solvents do not strongly interact with the NW, elements derived from shell precursors readily access the wire surface. This conclusion was corroborated by the need to strip bare NWs of TOPO and other strongly coordinating ligands with pyridine prior to overcoating. Coordinating solvents also potentially sequester precursor-derived elements, hindering shell growth. Interestingly, coordinating solvents have been used nearly exclusively in QD overcoating procedures. This difference in overcoating behavior may stem from the higher surface ledge density in spherical QDs than in NWs, which would, in turn, make adatom attachment easier, even in a coordinating environment.

A coordinating injection solution in conjunction with a noncoordinating NW solvent does, however, promote the overcoating of CdS/CdSe and CdSe/ZnTe NWs. In particular, TOP appears to limit the reaction rate such that shell growth occurs in a controlled fashion. By contrast, when the injection solution is completely noncoordinating (along with a noncoordinating NW solvent) the subsequent reaction proceeds much too rapidly, leading to poor-quality overcoatings with excess byproducts. Interestingly, reversing the procedure by using a coordinating NW solvent and a noncoordinating injection mixture causes reactions to fail. The exception to this trend is the CdSe/CdS synthesis, which only works when both injection and reaction solvents are noncoordinating.

Precursor injection rates and shell deposition temperatures also play a critical role in determining the quality of the resulting product. In particular, injection rates were varied between ~5 mL/h [200 (438) μmol/h metal (chalcogen)] to ~30 mL/h [1.2 (2.6) mmol/h metal (chalcogen)]. It was observed that slower injection rates led to better coatings as defined by smoother, more uniform surfaces, covering the entire NW length. By contrast, the rapid introduction of shell precursors resulted in uneven (patchy) coatings of poor quality. Optimal rates were therefore found empirically. We speculate that slow injection rates yield higher-quality shells because they maintain an overall low concentration of free precursor atoms in solution during the reaction. This ensures that a majority of these atoms react with the NW surface instead of self-nucleating to form QDs. In this sense, the behavior is qualitatively identical to overcoating colloidal QDs, where slow injection rates have generally yielded better overcoatings.[18−21]

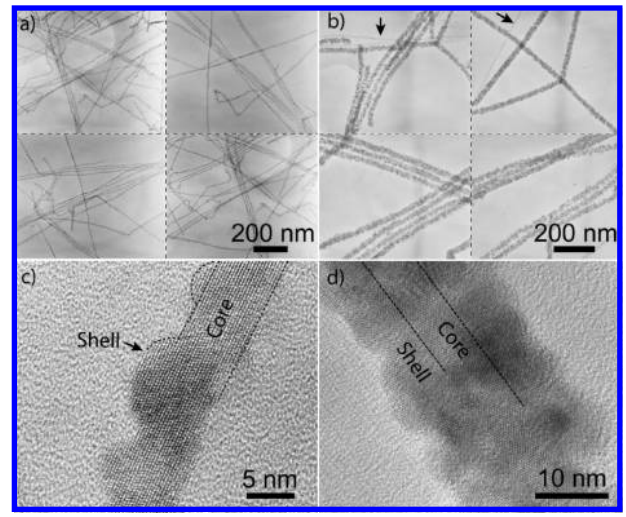

Figure 2. CdS/CdSe core/shell NWs with (a and c) thin (~1 nm) and (b and d) thick shells (~10 nm).

In tandem, optimal deposition temperatures depended upon precursor reactivity. To illustrate, the combination of $(TMS)_2Se$ [or $(TMS)_2S$] and $CdMe_2$ resulted in acceptable shell growth at temperatures as low as 215 °C for both CdS/CdSe and CdSe/CdS NWs. Slightly higher temperatures yielded even better coatings. As a consequence, ~240 °C was used in optimized preparations. By contrast, CdSe/ZnTe preparations utilizing $ZnEt_2$ and TBPTe, and CdS/CdSe preparations involving TOPSe, exclusively required these higher temperatures in order to obtain coatings of comparable quality. This implies that TOP- and TBP-based precursors are less reactive than their TMS counterparts. In all cases, temperature variations within 5 °C of optimal did not noticeably affect the quality of the resulting product.

These shell growth temperatures parallel trends with reported NC core/shell preparations. Whereas many QD overcoating schemes employ low reaction temperatures (100−150 °C[18,19]) to suppress Ostwald ripening, several studies have found that larger NCs require higher temperatures to achieve successful coatings.[19,22] Such behavior may be due to the large NC size, which should produce a lower ledge density and thus tend to inhibit shell growth. NW overcoating temperatures, ranging from 215 to 250 °C, are therefore in line with this trend given their relatively large core diameters and lower overall ledge densities.

3.2. Structural Characterization. 3.2.1. CdS/CdSe and CdSe/CdS. To better examine the structural and physical properties of resulting heterostructures, core/shell NWs were studied using low- and high-resolution electron imaging. Representative TEM micrographs of CdS/CdSe NWs are shown in Figure 2. A survey of such images reveals that ~95% of the wires appear coated, corroborating conclusions derived from previous SEM micrographs (Figure 1). Occasional uncoated wires can also be seen

(35) Brumer, M.; Kigel, A.; Amirav, L.; Sashchiuk, A.; Solomesch, O.; Tessler, N.; Lifshitz, E. *Adv. Funct. Mater.* **2005**, *7*, 1111.
(36) (a) Ivanov, S. A.; Piryatinski, A.; Nanda, J.; Tretiak, S.; Zavadil, K. R.; Wallace, W. O.; Werder, D.; Klimov, V. I. *J. Am. Chem. Soc.* **2007**, *129*, 11708. (b) Balet, L. P.; Ivanov, S. A.; Piryatinski, A.; Achermann, M.; Klimov, V. I. *Nano Lett.* **2004**, *4*, 1485. (c) Piryatinski, A.; Ivanov, S.; Tretiak, S.; Klimov, V. I. *Nano Lett.* **2007**, *7*, 108.

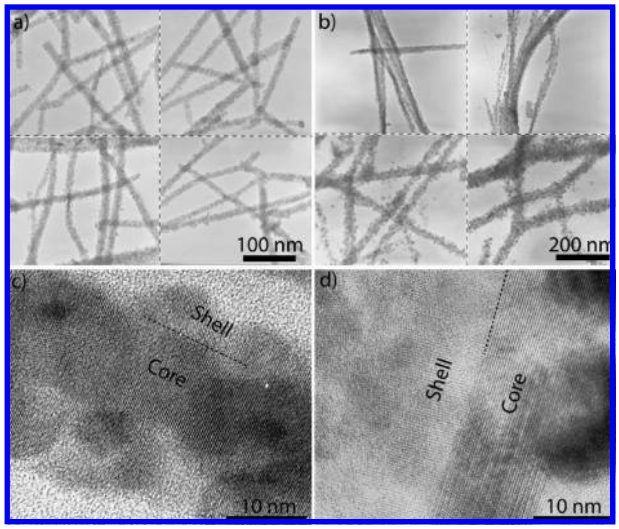

Figure 3. (a and b) Low-resolution TEM images of CdSe/CdS core/shell NWs. Images c and d show epitaxial growth at the outset with the appearance of polycrystalline growth at larger shell thicknesses.

and are most apparent in preparations where thick shells have been deposited (arrows, Figure 2b). Furthermore, low-resolution TEM images reveal relatively uniform shell growth across the entire NW length. In general, shell thickness variations range from 11% to 13% about the mean diameter (sample size, 20 wires), increasing to ~30% as the core NW diameter and corresponding shell thickness decreases (Figure 2c). By contrast, uncoated core NWs typically have intrawire diameter variations of 3−6%.[12]

In the thin-shell image in Figure 2c, the shell is clearly epitaxial with no misfit dislocations. Thus, instead of generating such defects during shell deposition, lateral strain relaxation of the growing islands must relieve most of the misfit strain present. Note that although there is no obvious image contrast between the CdS core and CdSe shell in Figure 2c, the islands were not present in the original core NWs (Supporting Information). Furthermore, the presence of Se was confirmed in the shell by EDXS.

By contrast, the thicker shell in Figure 2d is polycrystalline, exhibiting lattice fringes oriented in various directions. Thus, there exists a transition from epitaxial to nonepitaxial shell growth as the shell thickness increases. We surmise that, in Figure 2d, the islands have grown together and have coalesced and that the nucleation of new grains with random orientations has produced the polycrystalline part of the shell. In addition, in images such as Figure 2d where NWs have thicker shells, the presence or absence of misfit dislocations is difficult to judge due to the complex image formed by overlapping core and shell images.

Figure 3 shows TEM micrographs of resulting CdSe/CdS NWs. Low-resolution images reveal that the majority (~85%) of CdSe/CdS NWs in the ensemble are coated. Furthermore, coatings are relatively uniform with 10−14% shell thickness variations about the mean diameter (sample size, 20 wires). This increases to ~26% as the core NW diameter and corresponding shell thickness decreases. The texture of the system at large thicknesses appears similar to that of CdS/CdSe NWs, with a polycrystalline coat composed of numerous nanocrystallites.

In both CdS/CdSe and CdSe/CdS NWs, when thin shells (~1−3 nm thick) are deposited over the core, lattice fringes extend in the same orientation across the entire radial direction (Figures 2c and 3c). This implies a form of epitaxial shell growth at the outset of the deposition. In this regard, the bulk lattice mismatch (3.9%) between CdS and CdSe enables epitaxial shell growth, as previously noted for analogous CdSe/CdS core/shell QDs.[20]

In two-dimensional epitaxial thin-film growth on a flat substrate, the misfit strain energy in the film is proportional to thickness. This means that above a critical thickness it becomes energetically favorable for misfit dislocations to nucleate in order to relieve any strain.[37,38] Similar considerations apply to core/shell NWs or QDs, although the assumption that the epitaxial film does not strain the substrate would be modified because the shell thickness is not a negligible fraction of the NW core diameter. For thin film growth, a critical thickness of one or two monolayers is predicted for a lattice mismatch of 3.9%. However, at low temperatures it is possible to grow films many times this thickness without misfit dislocations. This is due to kinetic limitations for dislocation nucleation. Consequently, dislocation-free CdSe/CdS superlattices have been grown with thicknesses up to 5 nm.[39]

For epilayers with misfits of a few percent, island growth is an alternative way for the film to relieve strain. If the relative surface energies favor wetting of the substrate, several layers of the film grow epitaxially before nucleating three-dimensional islands: Stranski−Krastanov growth. If wetting is not favored, Volmer−Weber three-dimensional island growth is preferred without an initial epitaxial wetting layer. In the present study, Figure 3d shows an epitaxial layer which we take to be the Stranski−Krastanov wetting layer for CdS growth on CdSe. This is consistent with the observation of thin epitaxial shells in CdSe/CdS QDs.[20] It should be noted though that such uniform shells were observed only in a few cases. Figure 2c appears to be Volmer−Weber growth, consistent with the fact that reversing the core and shell materials favors wetting in one case (CdSe/CdS) and antiwetting in the other (CdS/CdSe). In both cases, thick shells are polycrystalline (Figure 2d and parts of 3d), indicating the nucleation of randomly oriented nanocrystals following island growth. Such shells have a high density of grain boundaries, containing bond length errors and dangling bonds which could, in turn, act as nonradiative recombination centers upon photoexcitation.

Analogous behavior has been observed with core/shell NWs made using vapor deposition. Specifically, instances of both epitaxial[23,24a] and polycrystalline[24b,26] shell growth have been observed. As an example of the former, highly epitaxial Si/Ge core/shell NWs have been made with shell thicknesses exceeding 10 nm despite a ~4.2% lattice mismatch.[24a] In the latter category, Si core/Si shell NWs have been made with fairly large shell thicknesses of approximately ~100 nm. However, despite the lack of a core/shell lattice mismatch, polycrystalline shells were observed.[24b]

3.2.2. CdSe/ZnTe. Figure 4 shows results from CdSe/ZnTe core/shell experiments. As can be seen, the ZnTe shell is not as uniform as coatings in comparable CdS/CdSe and CdSe/CdS preparations. Shell thickness variations of 21−24% about the mean diameter are seen (sample size = 20). This increases to ~26% with decreasing core diameter and corresponding shell thickness.

(37) Tu, K. N.; Mayer, J. W.; Feldman, L. C. *Electronic Thin Film Science for Electrical Engineers and Materials Scientists*; Macmillan, 1992.
(38) Matthews, J. W.; Blakeslee, A. E. *J. Cryst. Growth* **1974**, *27*, 118.
(39) Grun, M.; Hetterich, M.; Klingshirn, C.; Rosenauer, A.; Zweck, J.; Gebhardt, W. *J. Cryst. Growth* **1994**, *138*, 150.

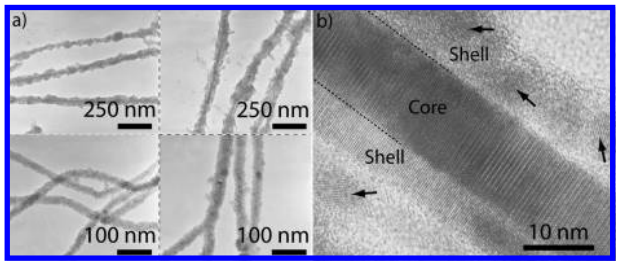

Figure 4. Corresponding (a) low- and (b) high-resolution TEM images of CdSe/ZnTe NWs. In (b), an extended crystalline section of the shell can be seen. Occasional crystalline domains (arrows) in other regions are also apparent.

Figure 4b illustrates a section of epitaxial shell growth over the CdSe core. This behavior is relatively uncommon since in most cases, much of the shell exhibits no lattice fringes apart from occasional nanocrystalline sections with randomly oriented lattice fringes (arrowed features, Figure 4b). However, selected area electron diffraction patterns reveal sharp rings that indicate the overall polycrystalline nature of the shell. By contrast, they are not strong and diffuse, as would be the case if it were amorphous. The general lack of lattice fringes in the ZnTe shell is thus attributed to it being in an orientation not suitable for lattice imaging. This is commonly seen when acquiring HRTEM images of core NWs.

The fact that the lattice mismatch between bulk CdSe and ZnTe is only ~0.8%[40] leads one to expect this system to be most amenable to epitaxial shell growth. The few examples observed therefore suggest that initial growth occurs via the Stranski−Krastanov mechanism, followed by subsequent nucleation of polycrystalline grains. Additional images of core NWs as well as corresponding core/shell species for all three systems can be found in the Supporting Information.

To further characterize core/shell NWs, EDXS analyses were conducted on all samples. Experiments were carried out at three spots along the length of each NW using a 25 nm spot. The large beam diameter was necessary in order to obtain an adequate signal from each point. Large NWs were therefore surveyed in an attempt to obtain approximate radial profiles of the element distribution. In the case of CdS/CdSe NWs, the overall wire diameter was on the order of the spot size. Therefore, analyses were performed on single core/shell NWs across their entire width.

Representative results of surveyed CdS/CdSe, CdSe/CdS, and CdSe/ZnTe NWs are shown in Figure 5. Locations where spot scans were acquired are circled with resulting average elemental compositions indicated. In all cases, errors in the acquired atomic percentages were ~1.5% for S, ~0.8% for Se and Cd, ~0.7% for Te, and ~1.2% for Zn.

Figure 5a displays representative results from CdS/CdSe wires, with each acquisition taken at the NW center. Although it was not possible to independently sample the composition of the shell, obtained (overall) mass ratios appear consistent with expected values based on apparent core/shell volumes. For example, in Figure 5a, given a core diameter of 10 nm and a corresponding shell thickness of approximately 9.4 nm, the estimated core (shell) NW volume is $V_{core} = 3.14 \times 10^{-16}$ cm^3/μm ($V_{shell} = 3.35 \times 10^{-16}$ cm^3/μm). With the use of bulk CdS and CdSe densities, the predicted CdS/CdSe mass ratio is then 1:1.26, comparing well with the obtained experimental value

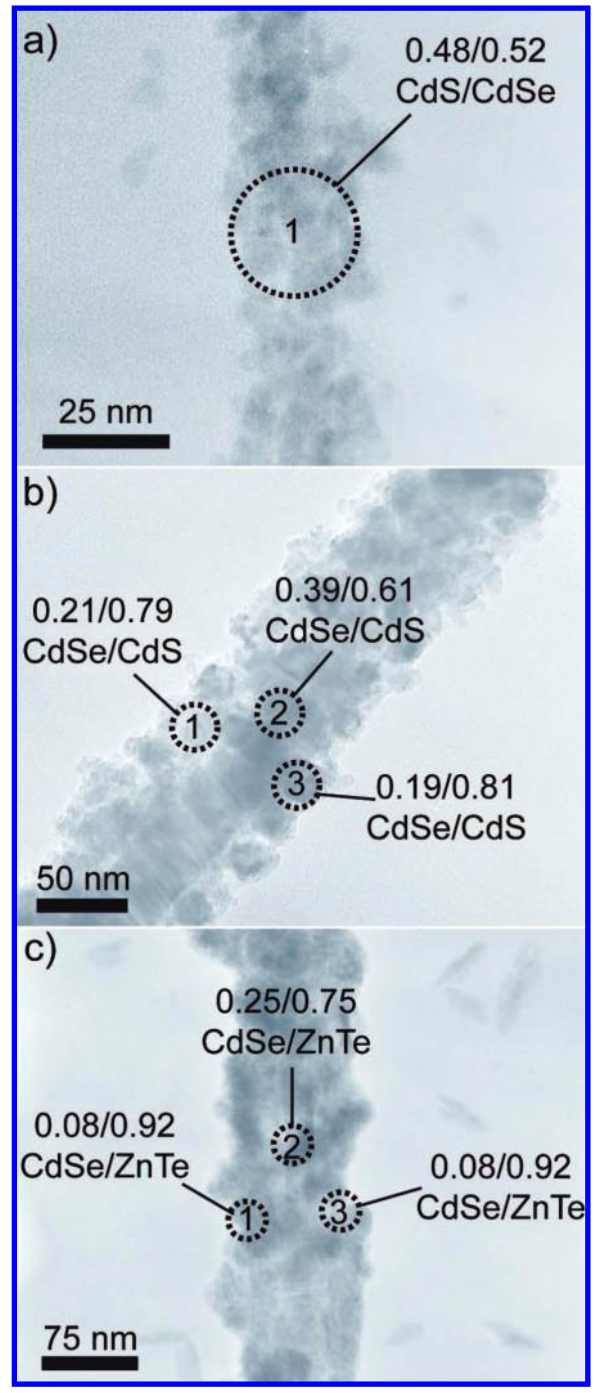

Figure 5. EDXS elemental analysis of (a) CdS/CdSe, (b) CdSe/CdS, and (c) CdSe/ZnTe core/shell NWs.

of 1:1.08. The comparison should be even better since the circular profile of the beam samples more of the core than the shell, skewing experimental numbers downward relative to calculated values.

Figure 5b displays analogous results for thicker CdSe/CdS NWs. Due to their larger diameters, it was possible to perform an analysis along their radial direction. The results clearly show NW edges containing a larger fraction of CdS to CdSe. This ratio reverses as one moves toward the core and the trend remains consistent among the multiple wires (six wires) surveyed. Identical EDXS analyses were performed on CdSe/ZnTe NWs (four wires) (Figure 5c), yielding analogous results.

(40) Xie, R.; Zhong, X.; Basche, T. *Adv. Mater.* **2005**, *17*, 2741.

As with CdSe/CdS, the composition of the coating consists predominantly of the intended shell material, ZnTe.

3.3. Optical Properties. An important reason for pursuing core/shell NWs is the modification of NW optical and electrical properties due to the presence of a semiconducting shell. As outlined earlier, core/shell NWs potentially exhibit type-I or type-II behavior based on bulk band offsets. Thus, depending on the actual offsets present, electrons and holes generated in the core can localize in either the core or the shell. This may then enhance NW photoluminescence QYs or enable the spatial separation of carriers into different parts of the heterostructure.[22,36] Furthermore, core/shell NWs offer the possibility of tuning dielectric contrast effects within core NWs. Thus, within the context of this study, overcoating NWs with another semiconductor may modify absorption/emission polarization anisotropies as well as 1D exciton binding energies, which could, in turn, enable more effective charge separation within NWs. In tandem, the strain induced by an overcoating may also modify the core NW band structure.[7−9] Since the optical properties of core/shell NWs have been largely unexplored, experiments were conducted on resulting CdS/CdSe, CdSe/CdS, and CdSe/ZnTe NWs.

3.3.1. Extinction Measurements. UV−vis extinction measurements of core/shell NWs are shown in Figure 6. The effect of coating CdS NWs with CdSe is apparent in Figure 6a through the growth of a prominent tail toward the red, ending at ∼710 nm, a value close to the bulk band gap of CdSe (712 nm, 1.74 eV). This tail originates from absorption by the CdSe shell. In this regard, the graph can be compared to the original CdS extinction spectrum, which has an absorption edge close to its bulk band gap (∼517 nm, 2.4 eV). Also of note, a shoulder also appears at ∼500 nm and results from absorption by the CdS core.

Given that the extinction spectrum shows both core and shell contributions, estimates were made for their respective absorption cross sections. With the use of core/shell NWs with the following dimensions, 10 nm diameter core, 5 nm shell thickness, absorption cross sections (σ_{abs}) were calculated at 387 and 500 nm.[33] The Supporting Information provides more details about these calculations. Note also that, formally speaking, these estimates are only valid at wavelengths far to the blue of the band edge where the NW density of states becomes bulklike. On the basis of actual comparisons between experiment and theory,[31] factor of 2 cross section differences at the band edge are easily possible. Obtained values were $\sigma_{CdS\ core\ 387nm} = 3.11 \times 10^{-11}$ cm^2/μm; $\sigma_{CdSe\ shell\ 387nm} = 8.36 \times 10^{-11}$ cm^2/μm, and $\sigma_{CdS\ core\ 500nm} = 1.03 \times 10^{-11}$ cm^2/μm; $\sigma_{CdSe\ shell\ 500nm} = 4.71 \times 10^{-11}$ cm^2/μm. These estimates suggest both core and shell contributions to the absorption throughout the visible.

Similar behavior can be seen with CdSe/CdS NWs. Although more difficult to discern shell contributions to the extinction because of overlapping CdS and CdSe spectra, two noticeable differences are seen in Figure 6b. Specifically, the extinction of coated NWs above >2.5 eV is larger than that of bare CdSe wires alone. This suggests the direct absorption of light by the shell. Theoretical estimates corroborate this, showing similar core/shell absorption cross sections at 387 and 500 nm [$\sigma_{CdSe\ core\ 387nm} = 6.26 \times 10^{-11}$ cm^2/μm; $\sigma_{CdS\ shell\ 387nm} = 5.58 \times 10^{-10}$ cm^2/μm and $\sigma_{CdSe\ core\ 500nm} = 3.53 \times 10^{-11}$ cm^2/μm; $\sigma_{CdS\ shell\ 500nm} = 1.85 \times 10^{-10}$ cm^2/μm] (15 nm diameter, 15 nm shell thickness). Furthermore, a slight (red) tail extends beyond the CdSe band edge, suggesting the delocalization of carriers into the shell as previously seen for analogous CdSe/CdS NCs.[20] The tail may also arise from scattering, but emission measurements in the subsequent section appear to confirm the above conclusion.

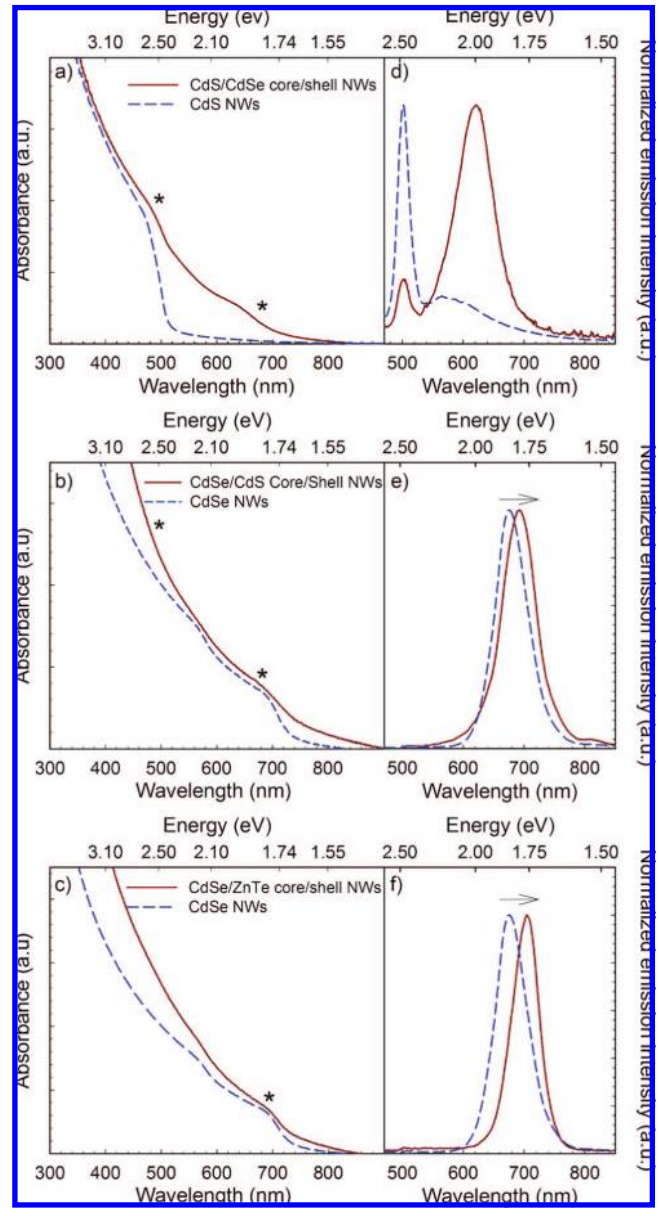

Figure 6. UV−vis extinction spectra of (a) CdS/CdSe, (b) CdSe/CdS, and (c) CdSe/ZnTe NWs. Asterisks denote wavelengths monitored in transient differential absorption measurements. Representative emission spectra of corresponding bare and overcoated (d) CdS/CdSe, (e) CdSe/CdS, and (f) CdSe/ZnTe NWs.

Identical UV−vis extinction measurements were conducted on CdSe/ZnTe NWs. Figure 6c shows that its spectrum is similar to that of bare CdSe wires. However, features of the CdSe core are dampened by the surrounding shell and appear less prominent. This is representative of all samples examined. Since the bulk band gap of ZnTe is 2.25 eV it should contribute a peak in the extinction at 525 nm, provided significant absorption cross sections. In this regard, calculated core/shell cross sections are $\sigma_{CdSe\ core\ 387nm} = 6.26 \times 10^{-11}$ cm^2/μm, $\sigma_{ZnTe\ shell\ 387nm} = 3.81 \times 10^{-10}$ cm^2/μm; $\sigma_{CdSe\ core\ 413nm} = 5.38 \times 10^{-11}$ cm^2/μm and $\sigma_{ZnTe\ shell\ 413nm} = 3.58 \times 10^{-10}$ cm^2/μm (15 nm core diameter, 15 nm shell thickness).

(33) Protasenko, V.; Hull, K. L.; Kuno, M. *Adv. Mater.* **2005**, *17*, 2942.

Despite these large values, only a featureless rise toward higher energies is seen in actual experiments. However, the extinction in the blue does tend to be larger than that of bare CdSe NWs alone, suggesting the absorption of incident light by the shell. In tandem, a red tail extends beyond the CdSe band gap and can be explained by the delocalization of carrier wave functions into the coating. Alternatively, it could result from the existence of a type-II heterojunction but would have to be proven within the context of other optical experiments. Scattering may also contribute to the tail, but a red-shifted emission seen in the next section argues against this and instead supports either of the two former explanations.

3.3.2. Emission Measurements. Complementary photoluminescence (PL) measurements were carried out on all samples. Representative spectra for thick core/shell NWs are shown in Figure 6d−f. In the majority of cases, a red-shift of the core emission maximum relative to the peak of the bare NW spectrum can be seen. This supports conclusions from above extinction measurements, suggesting delocalization of core carriers into the shell. Interestingly, Figure 6d shows a broad emission to the red of the core transition (∼500 nm) for both core (CdS) and core/shell (CdS/CdSe) NWs. In core wires, this likely stems from CdS surface defects, whereas in the latter core/shell species the red emission likely contains contributions from confined CdSe grains in the shell. This appears to be supported by the additional red-shift of the peak maximum while simultaneously maintaining an overall blue-shift relative to the bulk CdSe band gap. By contrast, no CdS shell emission is seen in Figure 6e.

QYs of uncoated CdS (CdSe) NWs have previously ranged from 0.068 to 0.95% (∼0.1%).[12d,33] In the current study, after multiple washings and exposure to pyridine bare NW QYs drop to ∼0.01%. Subsequent emission QY estimates of all core/shell species then yield values of ∼0.005% (CdS/CdSe), ∼0.02% (CdSe/CdS), and ∼0.001% (CdSe/ZnTe). Thus, although these core/shell QYs are not significantly different from each other an apparent trend can be seen. CdSe/CdS wires with a potential confining type-I potential exhibit larger QYs than their uncoated counterparts. Likewise, CdSe/ZnTe NWs exhibit relatively smaller QYs, suggesting potential type-II band offsets. In all cases, low overall core/shell QYs likely originate from misfit dislocations at the core/shell interface or from the existence of grain boundaries in the polycrystalline shell.

3.3.3. Transient Differential Absorption Measurements. Above extinction measurements have shown that both the core and the shell participate in the absorption of incident light. To explore any electronic interactions between the two, femtosecond transient differential absorption experiments were conducted. Both intraband and interband relaxation processes of the heterostructures were investigated by analyzing kinetics of the transient at different characteristic core/shell wavelengths. The potential existence of type-I or type-II band offsets may, in turn, be discerned by comparing the growth and decay bleach kinetics of coated NWs relative to their uncoated counterparts.

Transient differential absorption experiments were conducted by exciting core/shell NWs at 387 nm (3.20 eV). Excitation fluences ranged from 23.9 to 120 μJ/cm^2. Transient absorption spectra of NWs were subsequently acquired using a delayed, low-intensity white light continuum with wavelengths between 420 and 800 nm (2.95−1.55 eV). Bleach kinetics at 500 (2.48 eV) and 680 nm (1.82 eV), wavelengths corresponding to the effective band gaps of CdS and CdSe NWs, were, in turn, monitored. These spectral positions are denoted by asterisks in Figure 6. Furthermore, given previous extinction measurements and estimated cross sections, both the core and shell absorption/intraband relaxation were considered in subsequent data analyses.

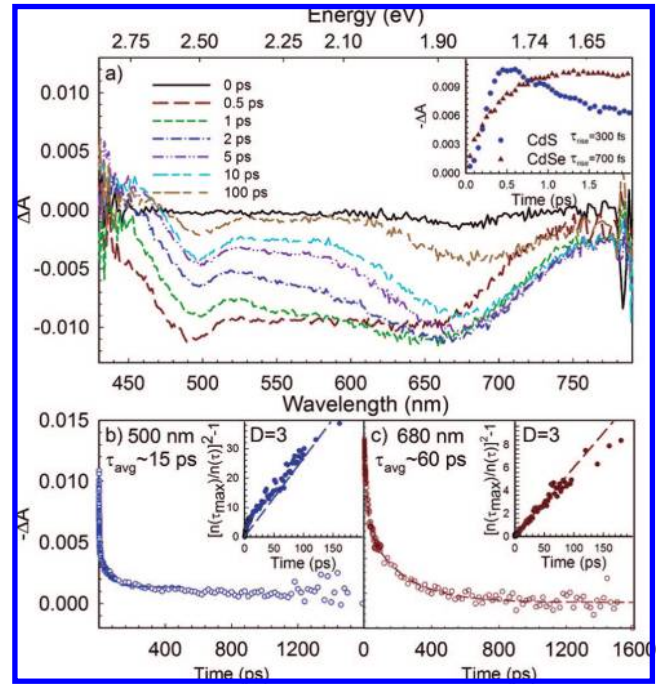

Figure 7. (a) Transient differential absorption spectra of CdS/CdSe core/shell NWs. The inset shows kinetics of the bleach growth at 500 and 680 nm, corresponding to the band edges of CdS and CdSe. (b) Subsequent decay kinetics at 500 and (c) 680 nm where dashed lines represent empirical fits to the data. Insets show three-carrier Auger fits to each trace.

Figure 7a shows transient absorption measurements performed on CdS/CdSe NWs (pump fluence = 59.7 μJ/cm^2). In the spectra, two transient bleaches are visible, one at ∼500 nm and another at ∼680 nm. These wavelengths correspond to the band gaps of CdS and CdSe and therefore likely represent contributions from the CdS core and CdSe shell. The claim is corroborated by the extinction spectra in Figure 6a. A broad featureless bleach is also observed between the two primary features and likely arises from rapid intraband relaxation within the CdSe shell, populating lower-lying states on the way to the band edge.

Focusing on the (core) CdS response, the induced bleach at 500 nm grows in and reaches a maximum within 0.5 ps (inset, Figure 7a). A fit to the experimental data shows an effective rise time of 0.3 ps and agrees well with previous values for the intraband relaxation rate in bare CdS NWs (∼0.3−0.4 ps).[12d] In parallel, the induced bleach at 680 nm (CdSe shell) grows in and reaches a maximum over 1.0 ps. The extracted 0.7 ps rise time is shorter than the ∼3 ps intraband recovery previously reported for bare CdSe NWs.[40] This implies the existence of another relaxation pathway that contributes to carrier population at the CdSe band edge, with the sum of rates yielding a shorter overall growth time. Within the context of an "inverted" type-I heterostructure, this faster growth can be explained by the migration of carriers from the core into the shell due to the existence of favorable band offsets (inset, Figure 1 and Supporting Information). Namely, a lower potential exists for both electrons and holes in the shell promoting their localization there.

The subsequent decay of the 500 nm transient was separately fit to a biexponential and exhibited a decay time scale of ∼15 ps (Figure 7b). This is shorter than previously reported for bare

CdS NWs (~1 ns).[12d] Along with the faster growth of the CdSe transient (above), it supports the migration of carriers into the CdSe shell. Alternatively, the faster decay could arise from the efficient nonradiative relaxation of carriers at core/shell defect states.

In principle, an Auger process could be expected in the core because bare CdS NWs have previously exhibited three-carrier Auger recombination kinetics at high carrier densities.[12d] This is supported by calculated core carrier densities on the order of $n(0) \sim 10^{19}-10^{20}$ cm^{-3} (Supporting Information). However, analyses of the data show that the 500 nm kinetics do not fit either a three-carrier ($D = 3$) or bimolecular ($D = 2$) Auger recombination process (inset, Figure 7b where D reflects the order of the kinetics). As a consequence, an apparent change in the Auger kinetics of the core appears to have been induced by the existence of a shell having potential type-I band offsets.

Decay kinetics of the CdSe shell were also examined (Figure 7c). The analysis reveals average 680 nm recovery time scales on the order of ~60 ps, which is shorter than previously observed for either CdSe QDs or NWs.[29,41] A gradual red-shift of the bleach is attributed to state filling as previously observed in CdS NWs.[12d]

Interestingly, the shell kinetics fit a three-carrier Auger process (inset, Figure 7c). This differs from the behavior of bare CdSe NWs where a bimolecular exciton−exciton annihilation process was previously observed at comparable pump fluences.[29] Assuming an Auger process, the discrepancy in the order of the shell recombination kinetics can be explained by the large number of uncorrelated carriers present in the shell due to carrier migration from the core. An alternate explanation, however, is that the polycrystalline nature of the coating leads to individual grains acting like QDs. These NCs, once excited, would then exhibit three-carrier Auger kinetics at high carrier densities. This latter explanation is supported by the blue-shifted (shell) emission spectra in Figure 6d, which suggests confinement effects in CdSe. The extracted experimental three-carrier Auger coefficient ($C_3 = 1.37 \times 10^{-29}$ cm^6/s), in either case, is in good agreement with reported literature values, ranging from $C_3 \sim 10^{-28}$ to $C_3 \sim 10^{-29}$ cm^6/s.[41]

The existence of a shell-localized three-carrier Auger process is further supported by the excitation intensity dependence of the data. Transient absorption studies were conducted with different pump fluences: 23.9, 59.7, and 120 μJ/cm^2 (corresponding spectra and kinetics, Supporting Information). Results from these experiments show reduced lifetimes at larger pump fluences where in all cases, the 680 nm transient obeys three-carrier Auger kinetics. An average C_3 coefficient of 6.04×10^{-29} cm^6/s ($\sigma = 8.89 \times 10^{-29}$ cm^6/s) is observed over the intensity range sampled.

Qualitatively similar behavior was observed in the transient differential absorption of CdSe/CdS NWs (pump fluence = 59.7 μJ/cm^2) (Figure 8). As before, transients were monitored at 500 and 680 nm (asterisks, Figure 6b). The broad featureless bleach between the two main features is again attributed to rapid intraband carrier relaxation within the CdSe core, populating intermediate states prior to the band edge. Since calculated CdSe core/CdS shell absorption cross sections at 387 nm have similar magnitudes, both core and shell intraband relaxation were considered in the analysis.

Obtained spectra show the 500 nm bleach growing in over 0.5 ps, with an obtained fit value of 0.3 ps. This agrees well

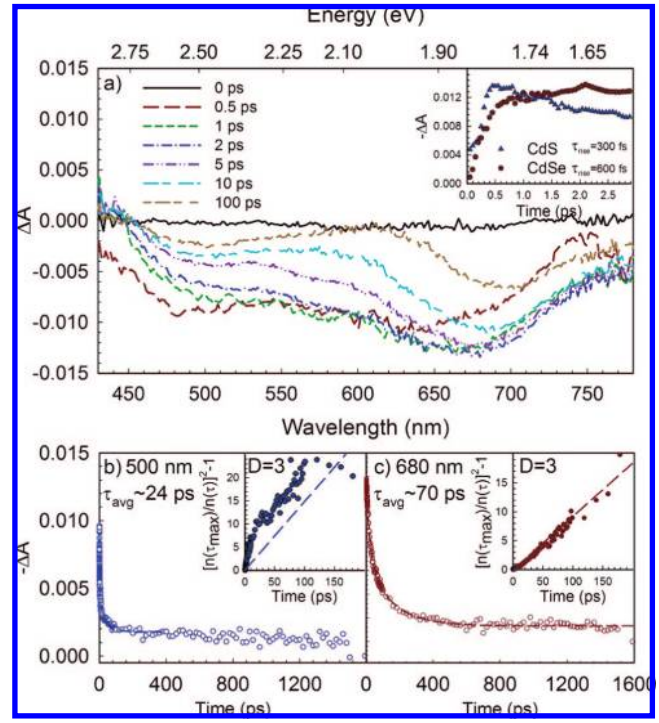

Figure 8. (a) Transient differential absorption spectra of CdSe/CdS core/shell NWs. The inset shows the signal rise at 500 and 680 nm. Corresponding kinetic data at (b) 500 and (c) 680 nm where dashed lines represent empirical fits. Insets show three-carrier Auger fits to the data.

with previous intraband relaxation time scales of bare CdS NWs (~0.3−0.4 ps).[12d] In tandem, the fitted rise of the 680 nm bleach is ~0.6 ps and is significantly faster than previously observed in bare CdSe NWs (~3 ps) (Figure 8a, inset).[29] The faster population of the core thus implies another carrier relaxation pathway, adding to any (core) intraband relaxation. Within the context of a type-I heterostructure, this faster growth can be explained by carrier migration from the CdS shell into the CdSe core with the sum of rates yielding faster overall growth times.

Subsequent decay of the 500 nm bleach occurs over ~24 ps (Figure 8b). This is much shorter than previously reported for bare CdS NWs (~1 ns) and can again be rationalized by carrier migration into the core. Alternatively, it can be explained by an increased contribution from nonradiative surface decay processes. However, the faster rise of the 680 nm bleach suggests the former. Notably, the decay kinetics of the 500 nm bleach do not fit either a bimolecular or a three-carrier Auger process (Figure 8b, inset).

In parallel, the 680 nm bleach decays over ~70 ps (Figure 8c), which is again much shorter than previously reported for bare CdSe NWs.[29] The gradual red-shift of the bleach is attributed to state filling as with the CdS/CdSe wires above. Interestingly, we find that these (core) decays exhibit third-order kinetics, characteristic of a three-carrier Auger process (Figure 8c, inset). This is supported by estimated (core) carrier densities on the order of $n(0) \sim 10^{19}$ cm^{-3} (Supporting Information). An average Auger coefficient over the range of pump fluences (23.9−120 μJ/cm^2) investigated is $C_3 = 4.27 \times 10^{-29}$ cm^6/s ($\sigma = 4.40 \times 10^{-29}$ cm^6/s) and agrees well with previously reported CdSe C_3 values.[41]

The interest in this observation is that bare CdSe NWs have previously been observed to exhibit second-order kinetics under near-identical pump fluences.[29] The absence of a suggested bimolecular exciton−exciton annihilation process, accompanied

(41) Klimov, V. I. *J. Phys. Chem. B* **2000**, *104*, 6112.

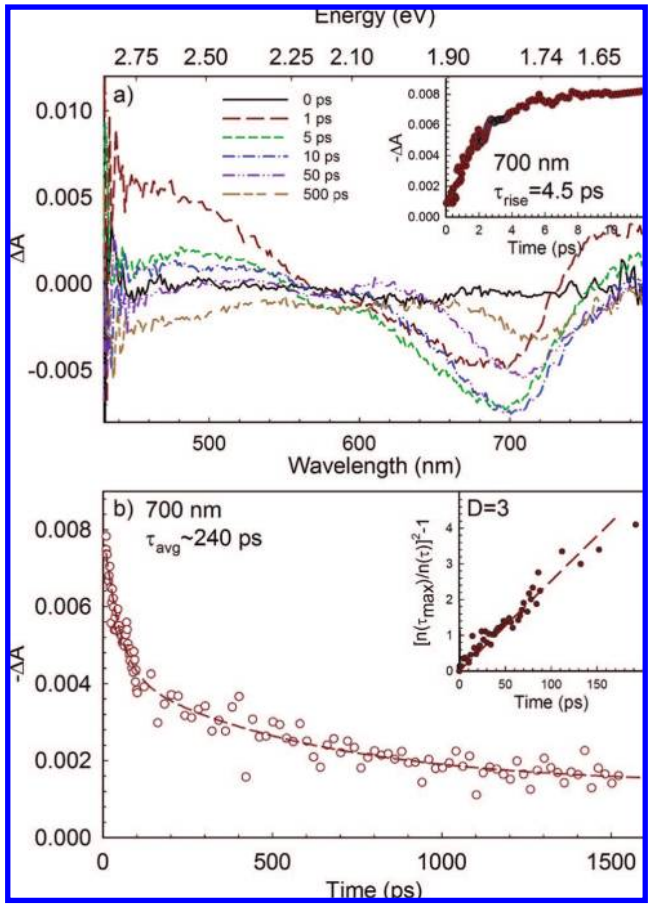

Figure 9. (a) Transient absorption spectra of CdSe/ZnTe core/shell NWs. The inset displays the growth of the 700 nm bleach. (b) Subsequent decay kinetics at 700 nm, with the dashed line being an empirical fit to the data. The inset shows a three-carrier Auger fit to the trace.

by a reversion to third-order kinetics, would then suggest that NW Auger kinetics can be manipulated by the introduction of a semiconductor shell. Specifically, the presence of core/shell band offsets could result in a large number of uncorrelated carriers within the core and might in turn, support a transition to three-carrier decay kinetics at high carrier densities.

Similar transient absorption measurements of CdSe/ZnTe NWs are shown in Figure 9 (pump fluence = 59.7 μJ/cm^2). However, the data appear more complicated. Expected is a transient absorption spectrum similar to that of bare CdSe NWs, with a bleach maximum around 680 nm. Also expected is a 525 nm bleach from the ZnTe shell due to its large estimated absorption cross section. In practice, a spectrum similar to that of bare CdSe NWs is observed with the main bleach at approximately 700 nm. No discernible contribution from the ZnTe shell can be seen. Although unexpected, this latter behavior is in line with the apparent absence of a ZnTe contribution to the linear absorption in Figure 6c. As a consequence, only core carrier dynamics are monitored in the subsequent analysis.

From the data, the 700 nm bleach grows in over ~4.5 ps. This is comparable to that previously reported for bare CdSe NWs (~3 ps).[29] Subsequent decay of the 700 nm bleach occurs over ~240 ps, which is longer than that observed with bare CdSe NWs (~130 ps) under similar excitation conditions. Within the context of a type-II heterostructure, longer interband decays can be rationalized by the spatial separation of electron−hole pairs at the band edge. The reduced electron and hole wave function overlap would then result in increased recombination times. Longer carrier lifetimes at the CdSe band edge are therefore suggestive. This conclusion, however, is by no means definitive and, in this regard, the ZnTe system appears more complicated than analogous CdS/CdSe and CdSe/CdS systems. A number of issues must therefore be resolved before making stronger conclusions about its behavior. For example, the induced absorption at wavelengths below 500 nm and above 700 nm in Figure 9a are not fully understood. Along with the lengthened band edge recovery, both point to the need for additional measurements beyond the scope of the current study.

Finally, core NW decays at various pump fluences fit apparent three-carrier Auger kinetics (inset, Figure 9b). This is opposed to the second-order bimolecular kinetics previously seen for bare CdSe NWs. The average Auger coefficient over the range of pump fluences studied is $C_3 = 4.26 \times 10^{-29}$ cm^6/s ($\sigma = 6.54 \times 10^{-29}$ cm^6/s) (Supporting Information) and agrees with previously measured three-carrier CdSe Auger coefficients[41] as well as with the average C_3 value extracted from CdSe/CdS NWs above. Such results again hint at the ability to influence core NW Auger kinetics by introducing a surrounding semiconductor shell.

4. Conclusions

The successful solution-phase synthesis of three core/shell NW systems with potential type-I and type-II band offsets has been demonstrated. By investigating different synthetic parameters, involving the coordinating nature of the reaction solvent, the precursor introduction rate, and the growth temperature, a qualitative understanding of the overcoating process was developed. Subsequent characterization shows evidence of Stranski−Krastanov growth through monolayer formation prior to island growth for CdSe/CdS and CdSe/ZnTe NWs. By contrast, initial CdS/CdSe shell growth appears to occur by Volmer−Weber island formation without a wetting layer. In either case, with increasing shell thickness, islands grow and impinge, after which the nucleation of randomly oriented grains forms a polycrystalline shell.

Core/shell electronic interactions were explored optically. Specifically, UV−vis extinction spectra and PL experiments show evidence of core/shell interactions through red-shifts in the absorption and emission. Both likely arise from delocalization of core-related carriers into the shell. Additional transient differential absorption experiments provide further insights into core/shell interactions through an analysis of carrier dynamics. Specifically, an additional carrier relaxation pathway from CdS into CdSe was observed for both CdS/CdSe and CdSe/CdS core/shell NWs, in line with expected type-I band offsets. More interestingly, Auger kinetics in core NWs were found to be altered by the presence of a semiconducting shell. Specifically, in CdSe NWs, the presence of a CdS shell changes the order of the Auger decay kinetics from second- to third-order. Likewise, in coated CdS NWs CdSe shells were observed to suppress previously seen three-carrier Auger kinetics. These observations may therefore ultimately enable one to better understand and possibly exploit the unique optical and electrical properties of semiconductor NWs.

Acknowledgment. We thank Kevin Tvrdy and Prashant Kamat for access and assistance with the use of the transient differential absorption spectrometer. We also thank Istvan Robel for a critical reading of the manuscript. M.K. thanks the NSF NER program

(ECS-0609172) for financial support. M.K. also thanks the University of Notre Dame, NSF CAREER program (CHE-0547784), the Notre Dame Radiation Laboratory, and the DOE Office of Basic Energy Sciences for partial financial support as well as access to their equipment and facilities. M.K. is a Cottrell Scholar of Research Corporation.

Supporting Information Available: Schematic energy diagram illustrating type-I and type-II band offsets for CdSe/CdS and CdSe/ZnTe NWs, table of bulk literature band offsets and accompanying references, theoretical NW absorption cross sections and molar concentrations, additional low- and high-resolution TEM images of core and core/shell NWs, calculated core carrier densities at a given pump fluence, detailed description of the Auger analysis, and pump fluence dependent transient differential absorption spectra for CdS/CdSe, CdSe/CdS, and CdSe/ZnTe NWs. This material is available free of charge via the Internet at http://pubs.acs.org.

JA805538P